Magnetic resonance imaging of the chest

Initial experience[1]

Jeffrey S. Ross., M.D.
Peter B. O'Donovan, M.D.
Gregory P. Borkowski, M.D.

Initial experience using magnetic resonance (MR) imaging of the chest is reported for 10 normal controls and 90 patients with a variety of thoracic pathologic conditions. MR is capable of imaging thoracic disease in the mediastinum and hili with greater inherent contrast than computed tomography because of the low-intensity signal produced by rapidly flowing blood and the tracheobronchial tree *versus* the high-intensity signal produced by mediastinal fat on images with short TE/TR times. Mediastinal and hilar adenopathy is readily apparent in MR images in the transverse, sagittal, or coronal planes. The mediastinal vasculature especially lends itself to MR imaging. The pulmonary parenchyma is difficult to image because of the effects of respiratory motion and long scan times (5–20 minutes). Cardiac and respiratory gating improve image quality, but at the expense of lengthening scan times. The final role that MR will have in thoracic imaging remains to be determined.

Index term: Thorax, magnetic resonance studies

Cleve Clin Q 52:533–539, Winter 1985

Computed tomography (CT) has been the premiere imaging modality for thoracic disease, especially for detecting hilar and mediastinal masses.[1–5] The configurations of the normal and abnormal pulmonary hili have been described in detail.[6–8] Dynamic CT scanning, coupled with bolus injections of intravenous contrast material, is capable of accurately defining mediastinal vasculature. However, the past two years have seen a surge of interest in the applications of magnetic resonance (MR) in chest imaging.[9–16] Since rapidly flowing blood produces no signal, the inher-

[1] Department of Radiology, The Cleveland Clinic Foundation. Submitted for publication March 1985; accepted May 1985. ht

0009-8787/85/04/0533/07/$2.75/0

Fig. 1. Sarcoidosis. Sagittal magnetic resonance image, TE 30/TR 500, shows hilar adenopathy (arrow).

ent contrast between the mediastinal soft tissues and the vasculature is greater than in CT. Images may be obtained not only in the transverse plane, but the sagittal and coronal planes as well, without relying on reformatting multiple image sections or changing patient positioning as in CT. In fact, any oblique plane may be imaged by MR without moving the patient but simply by rotating the magnetic field gradients. We present our initial experience with MR imaging of the chest in our first 100 subjects.

Basic principles

For a more detailed introduction into the principles of MR imaging, the reader is referred to several recent articles.[17–19] A brief description is presented below.

In hydrogen MR imaging, the single proton in the hydrogen nucleus can be likened to a tiny bar magnet. When placed into an external magnetic field (Bo), the protons tend to orient themselves along the magnetic field lines, with a small excess oriented with the field rather than against the field. This net magnetization vector (M) of the hydrogen protons can be moved from its equilibrium position along the magnetic lines of force (Z axis) by applying bursts of radiowaves into the sample. Depending upon the duration and strength of the radiofrequency (RF) pulse M can be tipped away from its equilibrium position into the x-y plane in any desired amount. An RF pulse that tips M 90 degrees from its equilibrium position is referred to as a 90-degree pulse.

In addition to behaving like bar magnets, hydrogen protons also exhibit spin, much like a spinning top. As M is tipped away from the Z axis into the x-y plane, the protons continue to rotate about the Z axis.

Following completion of the RF pulse the nuclei will return to their equilibrium position, characterized by two "relaxation times", T1 and T2. T1, or the "spin-lattice relaxation time", is the time for exponential growth of the Mz component of the magnetization back to its equilibrium value. After the initial RF pulse is applied, the protons tend to rotate about the Z axis in unison. T2, or the "spin-spin relaxation time", is characterized by the exponential decay of the Mx-y component or "dephasing" of the protons as they rotate about the Z axis.

Several pulsing sequences are available for imaging. Only the spin-echo (SE) technique will be discussed here. The spin-echo technique consists of a 90-degree RF pulse followed after a certain amount of time by a 180-degree RF pulse. The 180-degree pulse has the effect of reversing the dephasing that occurred because of magnetic field inhomogeneities, and the spontaneous echo signal is obtained. The time between the 90-degree pulse and the signal collection is termed the TE (time to echo) while the time between successive 90-degree RF pulses in an SE technique is the TR (time to repetition). To obtain an interaction between the RF pulse and M, the radiofrequency applied (f) must match the conditions set in the Larmor equation: $f = (\gamma/2\pi)$ Bo where γ is the gyromagnetic ratio unique for different MR-sensitive nuclei such as ^{1}H, ^{31}P, ^{19}F, or ^{23}N. Parameters that affect the MR signal intensity include proton density, T1 and T2 re-

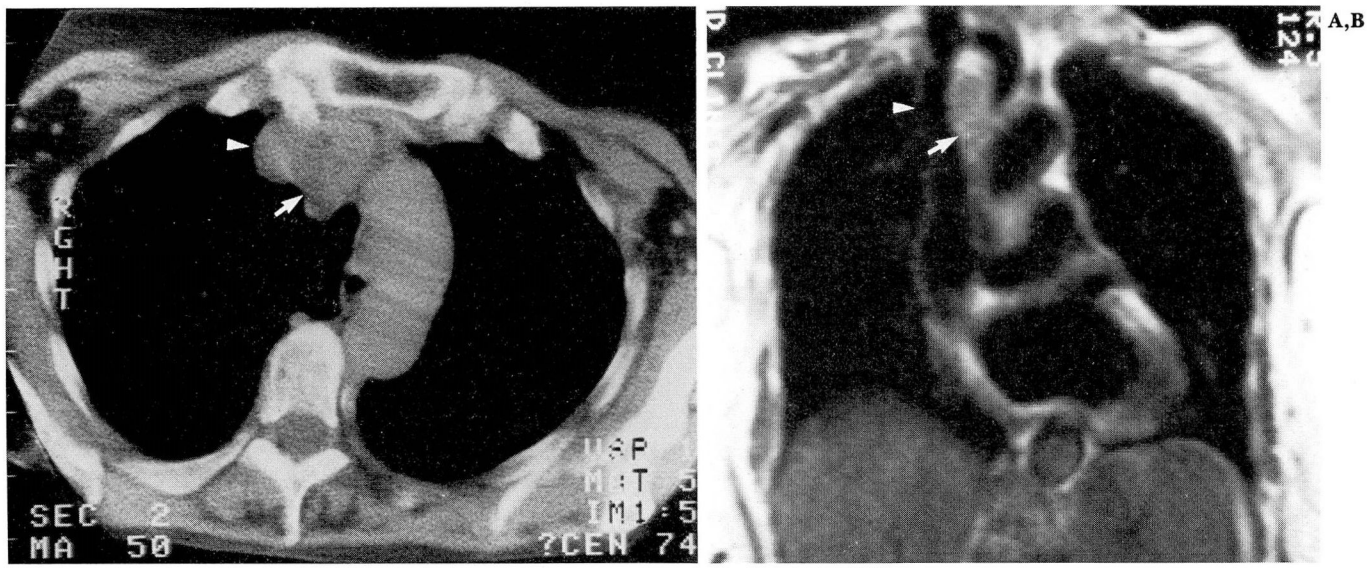

Fig. 2. Small-cell carcinoma.
A. CT scan shows adenopathy (arrow) medial to the superior vena cava (arrowhead).
B. Coronal magnetic resonance image, TE 30/TR 500, demonstrates the superior vena cava (arrowhead) and mediastinal adenopathy (arrow).

laxation times, and blood flow. The quantification of blood flow by MR has received considerable attention.[20–22] Rapidly flowing blood produces no MR signal because the moving protons in blood are within the section being imaged for such a short time that they do not receive the full complement of RF pulses. This effect has been termed the "flow void" phenomenon.[10]

Materials and methods

All images for this study were obtained upon a 0.6-Tesla superconducting magnet with 100-cm bore (Technicare Corporation, Solon, OH). Images were obtained with several different techniques as software was upgraded. Initially, single sections were imaged with a TE of 30 or 60 msec, a TR of 0.5 or 1 second, and a section thickness of 13 mm. Later, a multisection technique was used where up to 11 contiguous sections of a 1-cm thickness could be obtained with a TR of 0.5 sec. Finally, image thickness was decreased to 4 mm with the latest software. TE times could be varied among 30, 60, 90, or 120 msec. The number of signal averages varied from 2–6, depending upon the axis of imaging. The majority of coronal and sagittal scans used four signal averages. Cardiac gating, where the TR is fixed in relation to the RR interval, was used in 24 patients. Combined respiratory and cardiac gating was used in 20 patients. Forty-six patients did not have gated imaging.

Written informed consent was obtained from all subjects. Pregnant women, children under 2 years of age, and patients with cardiac pacemakers were excluded from this study.

Results

Ninety patients with suspected pulmonary abnormalities were imaged between September 1983 and November 1984. Ten normal volunteers were used as control subjects. Subjects imaged included 39 with bronchogenic carcinoma, eight with metastatic disease, five with esophageal carcinoma, five with benign mediastinal masses, and a variety of other pathologic conditions.

Hili

The normal appearance of the hili by MR has been described by Webb et al[13,15] for the transverse plane and by O'Donovan et al[20] for the coronal and sagittal planes. The greatest strength of MR imaging in chest disease is the clarity with which this modality demonstrates hilar abnormalities. Normally, little signal arises from the hili because of the lack of signal from rapidly flowing blood in the vasculature and air within

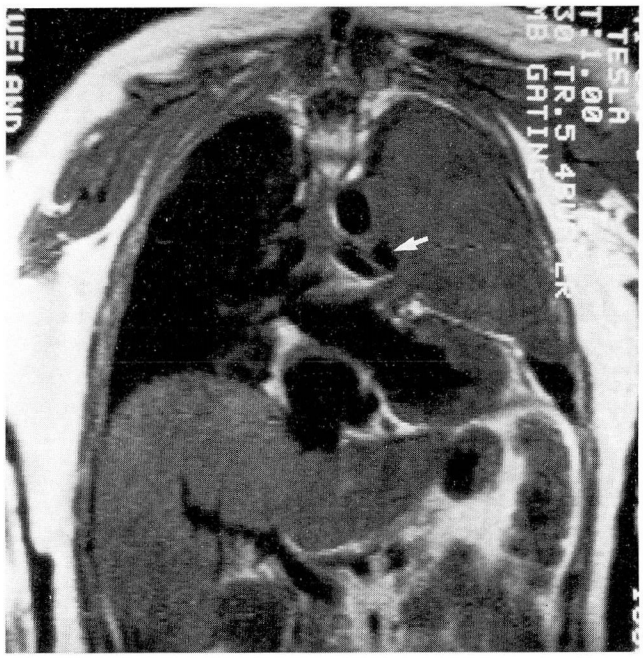

Fig. 3. Malignant fibrous histiocytoma. Coronal magnetic resonance image, TE 30/TR 500, shows compression of the left pulmonary artery (arrow) by a soft-tissue mass occupying the left hemithorax.

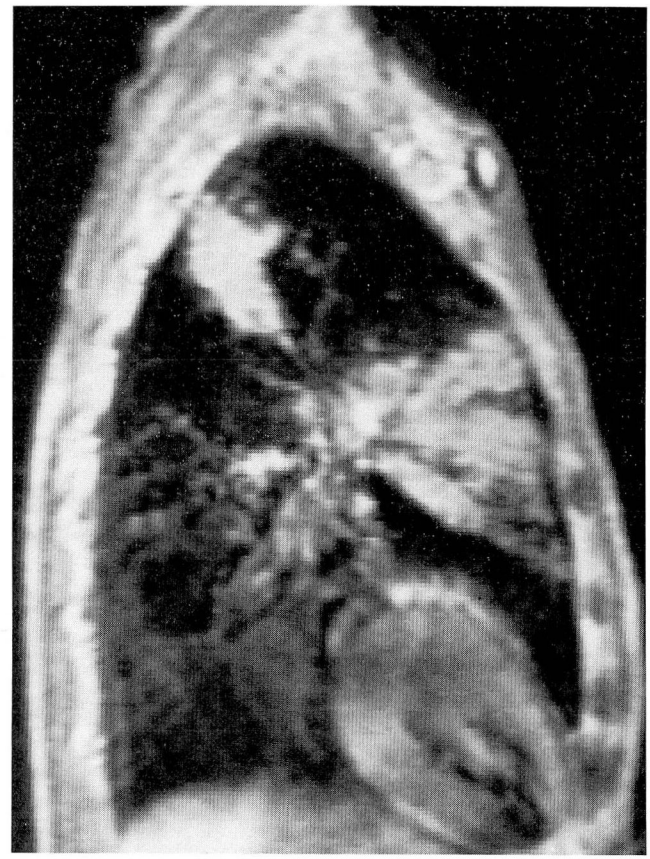

Fig. 4. Silicosis. Sagittal magnetic resonance image, TE 30/TR 500, shows conglomerate masses of intermediate signal intensity.

the tracheobronchial tree. Abnormalities are readily recognized as discrete areas of signal production. The sagittal plane can be especially valuable for detecting hilar disease since adenopathy in this plane is seen as rounded masses outlined against the pulmonary parenchyma, which appears dark because of low proton density. *Figure 1* shows a patient with sarcoidosis. The right hilar adenopathy is well seen in the sagittal plane.

Mediastinum

Like the hili, the mediastinum lends itself to MR imaging because the ability to image sagittal and coronal sections complements the vertical orientation of the mediastinal vasculature. Also, the mediastinum tends to be less affected by respiratory and cardiac motion degradation. However, the addition of cardiac and respiratory gating has significantly improved overall image quality, even that of the mediastinum. The lack of signal from the mediastinal vasculature is contrasted with the relatively high signal intensity (short T1) of the mediastinal fat and areolar tissue. Mediastinal tumors or adenopathy are generally seen as masses of intermediate signal intensity on short TE/TR images (*Fig. 2*).

Because of the lack of signal from flowing blood, the effect of mediastinal masses on the vasculature is easily assessed by MR without intravenous contrast material. Cohen et al[10] describe the MR findings in superior vena caval obstruction. Webb et al[13] have reported the ability of MR to demonstrate mediastinal lymphadenopathy and its relation to normal surrounding structures in the sagittal and coronal planes. We have found MR useful in the preoperative evaluation of patients undergoing laser photoresection of endobronchial lesions to determine the relationship of the lesions to surrounding mediastinal vasculature (*Fig. 3*). Sagittal and coronal images facilitate the demonstration of these anatomic relationships to a better advantage than axial CT images in many cases (Ross, unpublished data).

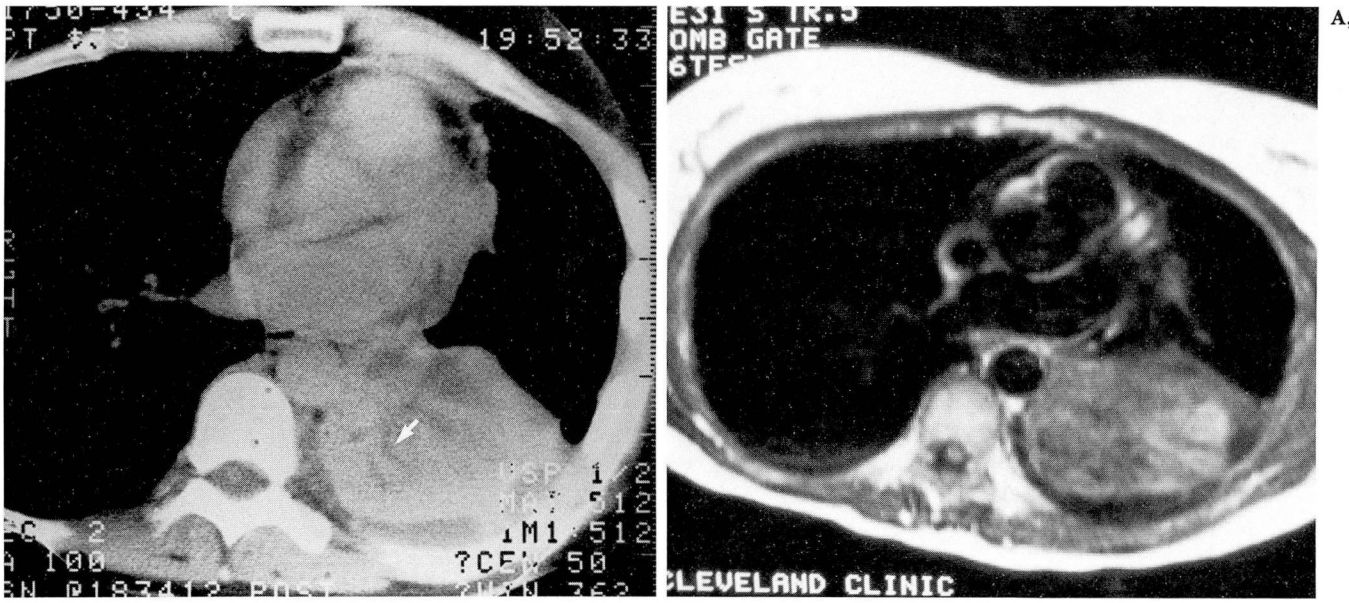

Fig. 5. Squamous-cell carcinoma.
A. CT scan shows left lower lobe collapse with a small pleural effusion. Fluid-filled bronchi are visible (arrow).
B. Transverse magnetic resonance image, TE 31/TR 500, at the same level shows similar findings.

Pulmonary parenchyma

The pulmonary parenchyma is a difficult area for MR imaging. Cardiac and respiratory motion, combined with the long scan times (4 to 20 minutes) and low proton density of the parenchyma, make visualization of parenchymal details difficult. Just as gating is helpful in the mediastinum and hili, combined respiratory and cardiac gating relieves some of the motion degradation problems of imaging the pulmonary parenchyma.

The recognition of an interstitial infiltrate appears partly dependent upon the size of the nodular component. Small, 2–3-mm nodules, as are present in early silicosis, cannot be visualized with current technology. Larger masses are seen as intermediate signal intensity on short TE/TR scans (*Fig. 4*). Pulmonary fibrosis can be seen as either a reticular pattern or a homogeneous area of medium signal intensity. Consolidated lung shows medium signal intensity on short TE/TR images, which can contain areas of decreased signal intensity representing fluid-filled bronchi (*Fig. 5*). Air bronchograms may also be seen in consolidated lung. The fissures are seen as areas of almost no signal production.[20]

Because of the problem of respiratory motion and long scan times, peripheral neoplasms cannot be visualized unless they are larger than approximately 1.5 cm in diameter. Cavitation can be visualized as areas of decreased signal production, such as within a neoplasm or abscess[12] (*Fig. 6*).

Pleura and chest wall

Pleural effusions are most often seen as areas of low signal intensity on short TE/TR images (long T1 and T2 values) in the dependent portions of the thorax, as in CT (*Fig. 5*). Occasionally, the signal from an effusion will be so low that pneumothorax would be suggested.[16] Benign pleural thickening is seen as thin plaques of intermediate signal intensity along the pleural surface. These are most apparent in the sagittal plane.

Since calcium does not produce an MR signal, subtle cortical bone involvement of the ribs by neoplasm cannot be assessed. The position of the ribs is apparent on MR images by the location of the high-signal-producing fat residing within the marrow. Also, dystrophic calcification within tumor masses or pleural calcifications, as seen in asbestosis, is not visible by MR. Involvement of the soft tissues of the chest wall can, however, be visualized on MR by noting the disruption of the tissue planes of the chest wall as well as the tumor mass itself. *Figure 7* is a case of plasmacytoma.

A,B

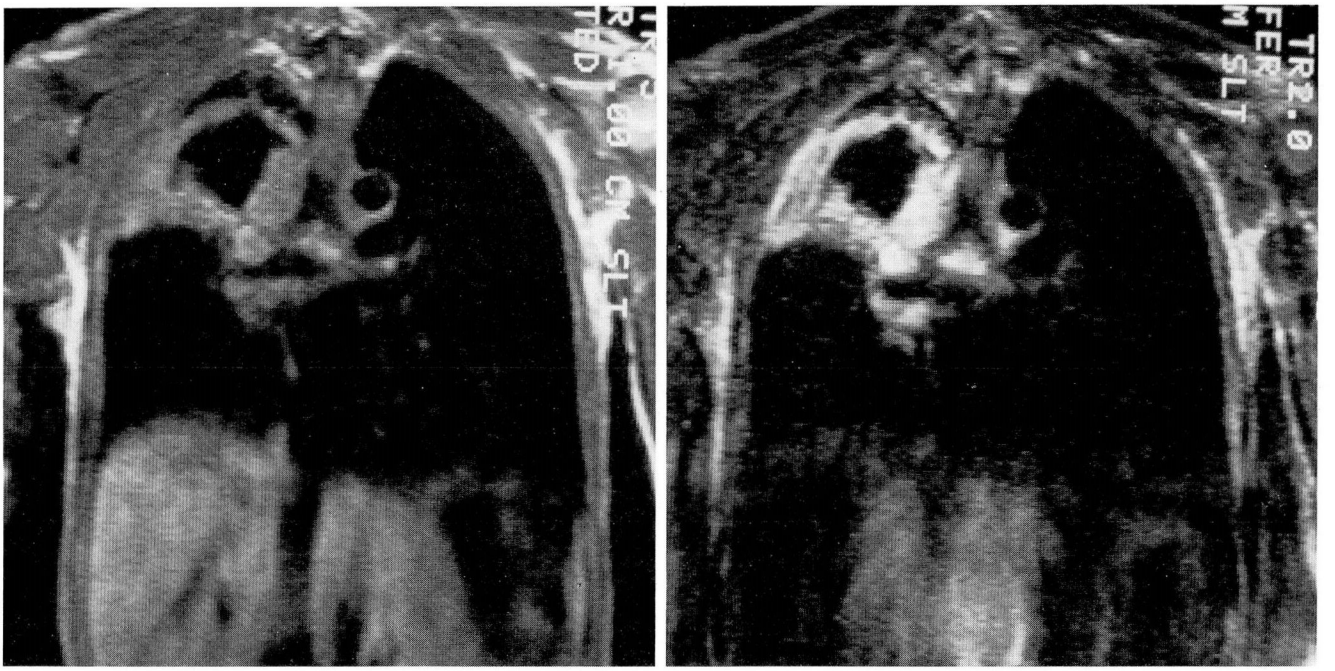

Fig. 6. Cavitated non-small-cell carcinoma.
A. Coronal magnetic resonance image, TE 30/TR 500, shows large cavitated mass in the right upper lobe.
B. Coronal magnetic resonance image, TE 90/TR 2000, shows increased signal intensity from the mass.

The tumor can be seen extending into the base of the neck on the sagittal MR image.

Discussion

MR imaging is capable of providing excellent anatomic detail of the mediastinum and hili, not only in a transverse plane but in the sagittal and coronal planes as well. MR does not use ionizing radiation, and intravenous contrast material is not necessary to achieve good contrast between the vasculature and the mediastinal and hilar tissues. MR has the potential to give not just anatomic detail but physiologic data as well, in the form of MR spectroscopy.

Conversely, the resolution of MR has not yet achieved that of CT. MR scan times can be long, ranging up to 20 minutes. Calcium is not visualized by MR. MR examinations of the chest are more susceptible to image degradation by cardiac and respiratory motion than are those of CT. Cardiac and respiratory gating will alleviate some of the motion degradation, but this also increases the length of the scan time by a factor of two or more.

MR has proved itself capable of defining normal and abnormal anatomy in the chest. However, the role that this new modality will have in relation to plain radiography, radionuclide imaging, and CT in chest disease remains unanswered.

Peter B. O'Donovan, M.D.
The Cleveland Clinic Foundation
9500 Euclid Avenue
Cleveland, OH 44106

References

1. Crowe JK, Brown LR, Muhm JR. Computed tomography of the mediastinum. Radiology 1978; **128:**75–87.
2. Osborne DR, Korobkin M, Ravin CE, et al. Comparison of plain radiography, conventional tomography, and computed tomography in detecting intrathoracic lymph node metastases from lung carcinoma. Radiology 1982; **142:**157–161.
3. Webb WR, Gamsu G, Glazer G. Computed tomography of the abnormal pulmonary hilum. J Comput Assist Tomogr 1981; **5:**485–490.
4. Webb WR, Gamsu G, Speckman JM. Computed tomography of the pulmonary hilum in patients with bronchogenic carcinoma. J Comput Assist Tomogr 1983; **7:**219–225.
5. Sone S, Higashihara T, Morimoto S, et al. CT anatomy of hilar lymphadenopathy. AJR 1983; **140:**887–892.
6. Webb WR, Glazer G, Gamsu G. Computed tomography of

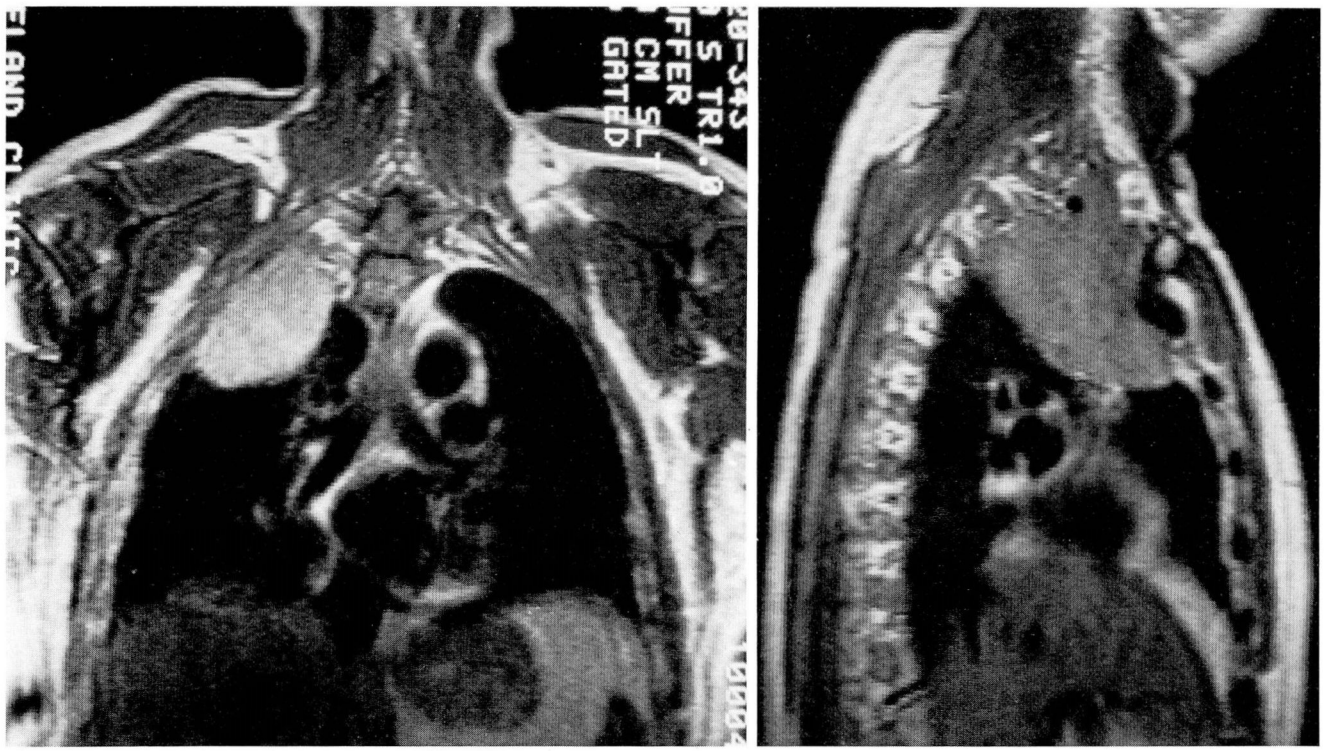

Fig. 7. Plasmacytoma. Coronal (**A**) and sagittal (**B**) magnetic resonance images, TE 30/TR 500, show a large mass in the right lung apex extending into the base of the neck.

the normal pulmonary hilum. J Comput Assist Tomogr 1981; **5:**476–484.
7. Naidich DP, Terry PB, Stitik FP, Siegelman SS. Computed tomography of the bronchi: 1. Normal anatomy. J Comput Assist Tomogr 1980; **4:**746–753.
8. Naidich DP, Stitik FP, Khouri NF, Terry PB, Siegelman SS. Computed tomography of the bronchi. 2. Pathology. J Comput Assist Tomogr 1980; **4:**754–762.
9. Gamsu G, Webb WR,, Sheldon P, et al. Nuclear magnetic resonance imaging of the thorax. Radiology 1983; **147:**473–480.
10. Cohen AM, Creviston S, LiPuma JP, et al. Nuclear magnetic resonance imaging of the mediastinum and hili: early impressions of its efficacy. AJR 1983; **141**;1163–1169.
11. Axel L, Kressel HY, Thickman DM, et al. NMR imaging of the chest at 0.12 T: initial clinical experience with a resistive magnet. AJR 1983; **141:**1157–1162.
12. Brasch RC, Gooding CA, Lallemand DP, Wesbey GE. Magnetic resonance imaging of the thorax in childhood. Radiology 1984; **150**:463–467.
13. Webb WR, Gamsu G, Crooks LE. Multisection sagittal and coronal magnetic resonance imaging of the mediastinum and hila. Radiology 1984; **150:**475–478.
14. Gamsu G, Stark DD, Webb WR, Moore EH, Sheldon PE. Magnetic resonance imaging of benign mediastinal masses. Radiology 1984; **151:**709–713.
15. Webb WR, Gamsu G, Stark DO, Moore EH. Magnetic resonance imaging of the normal and abnormal pulmonary hila. Radiology 1984; **152:**89–94.
16. Ross JS, O'Donovan PB, Novoa R, et al. Magnetic resonance of the chest: initial experience with imaging and *in vivo* T1 and T2 calculations. Radiology 1984; **152:**95–101.
17. Curry TS, Dowdey JR, Murry RC, Jr. Christensen's Introduction to the Physics of Diagnostic Radiology. 3rd edition. Philadelphia, Lea and Febiger, 1984, pp 461–503.
18. Partain CL, James AE, Rolo FD, Price RR, eds. NMR Imaging. Philadelphia, W.B. Saunders Company, 1983, pp 45–106.
19. Nuclear magnetic resonance: principles of imaging, pulse sequences, equipment, and clinical applications. Radiographics 1984; **4**.
20. O'Donovan PB, Ross JS, Sivak ED, O'Donnell JK, Meaney TF. Magnetic resonance imaging of the thorax: the advantages of coronal and sagittal planes. AJR 1984; **143:**1183–1188.
21. Mills CM, Brant-Zawadzki M, Crooks LE, et al. Nuclear magnetic resonance: principles of blood flow imaging. AJR 1984; **142:**165–170.
22. Crooks LE, Mills CM, Davis PL, et al. Visualization of cerebral and vascular abnormalities by NMR imaging; the effects of imaging parameters on contrast. Radiology 1982; **144:**843–852.
23. George CR, Jacobs G, MacIntyre WJ, et al. Magnetic resonance signal intensity patterns obtained from continuous and pulsatile flow models. Radiology 1984; **151:**421–428.
24. Kaufman L, Crooks LE, Sheldon PE, Rowan W, Miller T. Evaluation of NMR imaging for detection and quantification of obstruction in vessels. Invest Radiol 1982; **17:**554–560.